Research Article

Journal of Environmental Nanotechnology

Biogenic SiO_2 Nanoparticles Derived from Diatomaceous Biosludge for Sub-ambient Radiative Cooling Geopolymer Coatings

S. Gayathri[1], A. Swetha[2], Arun Kumar[3], M. K. Muniyasamy[4*], S. Premkumar[5] and G. Pavithra[6]

[1]Department of Civil Engineering, Vignan's Institute of Information Technology, Duvvada, Vishakapatnam, AP, India
[2]Department of Civil Engineering, Deccan College of Engineering and Technology, Nampally, Hyderabad, TG, India
[3]Department of Chemistry, Jaya Sakthi Engineering College, Chennai, TN, India
[4]Department of Civil Engineering, Saveetha School of Engineering, Saveetha Institute of Medical and Technical Sciences, Chennai, TN, India
[5]Department of Civil Engineering, Rajalakshmi Engineering College, Chennai, TN, India
[6]Department of Electronics and Communication Engineering, Dayananda Sagar College of Engineering, Bangalore, KA, India
Received: 18.02.2026 Accepted: 25.02.2026 Published: 30.03.2026
*munishcivilian1@gmail.com

ABSTRACT

The development of non-polymeric, environmentally resilient radiative cooling materials is critical for reducing passive heat loads in buildings. This study reports the novel use of biogenic SiO_2 nanoparticles derived from diatomaceous biosludge as multifunctional modifiers for geopolymer-based radiative cooling coatings. The biosludge-derived silica was processed into nanoscale SiO_2 and functionalized using 3-aminopropyltriethoxysilane (APTES) to improve dispersion and interfacial compatibility within the geopolymer matrix. Three systems were investigated: a plain geopolymer, a geopolymer with unfunctionalized biogenic nano-SiO_2, and a geopolymer with APTES-functionalized biogenic nano-SiO_2. Characterization (XRD, FTIR, SEM/EDX, TGA, UV–Vis–NIR, and infrared emissivity) revealed that biogenic nano-SiO_2 actively participated in geopolymer gel formation, refining the pore structure and improving thermal stability. APTES-functionalized biogenic SiO_2 produced the most pronounced improvements, yielding a densely crosslinked aluminosilicate matrix with enhanced broadband solar reflectance (~36%), near-unity infrared emissivity (8–13 μm), and the highest compressive strength (32.4 MPa). Outdoor field measurements confirmed that the APTES-functionalized coating consistently achieved 2–3 °C sub-ambient daytime cooling under direct solar exposure, whereas the plain geopolymer exhibited above-ambient temperatures. These results demonstrate that waste-derived, surface-functionalized biogenic silica provides a sustainable, scalable route for tuning the structural and optical properties of geopolymers for passive thermal management.

Keywords: Geopolymer coatings; Radiative cooling; Biogenic SiO_2 nanoparticles; Diatomaceous biosludge; APTES functionalization; Infrared emissivity; Solar reflectance; Sustainable materials; Passive cooling.

1. INTRODUCTION

The rapid growth in global energy consumption associated with space cooling has created an urgent need for materials capable of reducing thermal loads without relying on electricity-driven systems. Buildings alone account for nearly 40% of worldwide energy use, a significant portion of which is dedicated to air-conditioning technologies that rely heavily on fossil-derived electricity sources (Hitchin, 2019). As urban populations continue to expand and climate patterns shift towards more extreme temperatures, passive cooling technologies have gained increasing attention as a sustainable alternative to conventional cooling strategies (Hughes *et al.* 2011; Li *et al.* 2017; Chetan *et al.* 2020). Among them, sub-ambient daytime radiative cooling (SDRC) has emerged as a promising technique capable of lowering surface temperatures below ambient values under direct sunlight, without any external energy input (Li *et al*. 2020). SDRC materials achieve cooling by reflecting incident solar radiation while simultaneously emitting thermal radiation through the atmospheric transparency window (8–13 μm) into outer space (Gao and Chen, 2023). Although impressive progress has been made through photonic structures and metamaterials capable of selective spectral control, such systems often require complex fabrication processes, vacuum deposition, or metallic back reflectors, all of which hinder large-scale application due to cost and durability concerns (Griffith *et al.* 2015). This challenge has motivated the exploration of inorganic coating systems that can be produced at low cost, applied using conventional coating techniques, and exhibit long-term stability under harsh environmental conditions. In this regard, geopolymers—inorganic aluminosilicate binders formed by the alkaline activation of kaolinitic or industrial aluminosilicate precursors—are particularly attractive (Kryvenko *et al.* 2024). Their three-dimensional, amorphous aluminosilicate framework provides high chemical resistance, inherent fire

resistance, and environmental benefits due to the absence of Portland clinker production (Vignesh *et al.* 2025). More importantly, geopolymers possess intrinsic high infrared emissivity due to Si–O–Al vibrational modes, which naturally coincide with the atmospheric window, making them promising candidates for radiative cooling coatings (Liu *et al.* 2025). However, the solar reflectance of unmodified geopolymers remains insufficient for efficient daytime cooling, primarily due to their limited capacity to scatter incoming solar radiation.

Recent studies show that incorporating optically active fillers such as TiO_2, Al_2O_3, and $BaSO_4$ enhances solar reflectance in geopolymers through Mie scattering (Veloso *et al.* 2021; Ziada *et al.* 2025). However, these fillers interact merely physically with the matrix. Silica nanoparticles (SiO_2), conversely, offer high surface area and chemical reactivity, allowing them to participate directly in geopolymer gel formation. This refines pore structure and simultaneously improves solar reflectance and infrared emissivity. Because pristine SiO_2 nanoparticles tend to agglomerate, surface functionalization with silane coupling agents such as 3-aminopropyltriethoxysilane (APTES) is necessary to ensure stable dispersion and robust interfacial bonding (Si–O–Si) within the highly alkaline geopolymer environment (Jagajeevan and Sivakumar, 2026). Despite these advantages, the combined influence of functionalized nanoparticles on the optical, structural, and sub-ambient cooling performance of geopolymer binders remains underexplored. An additional and largely unexplored opportunity lies in the use of waste-derived biogenic silica as an alternative to synthetic nanosilica. Diatomaceous biosludge, a by-product of wastewater treatment processes, represents an abundant and under-utilized source of amorphous biogenic SiO_2. Unlike industrial silica, biogenic silica possesses a hierarchically textured surface, intrinsic disorder, and high chemical reactivity, which can enhance dissolution and polycondensation behavior in alkaline environments. Integrating such waste-derived nanosilica into geopolymer matrices not only improves material performance but also aligns radiative cooling technologies with circular economy and sustainable construction principles. To address this gap, the present study investigates the role of unfunctionalized and APTES-functionalized biogenic SiO_2 nanoparticles derived from diatomaceous biosludge (DE-SiO_2) in enhancing the radiative cooling performance of geopolymer coatings. Three systems were prepared: (i) plain geopolymer, (ii) geopolymer modified with pristine SiO_2 nanoparticles, and (iii) geopolymer modified with APTES-functionalized SiO_2 nanoparticles. Comprehensive characterization was conducted to examine their optical performance (solar reflectance and infrared emissivity), structural evolution (XRD, FTIR), microstructure (SEM), thermal stability (TGA–DTA), and mechanical properties. Field testing was also performed to quantify sub-ambient cooling performance under natural climatic conditions. The outcomes of this study provide key insights into the structure–property–performance relationships governing nanoparticle-modified geopolymers and demonstrate the potential of functionalized silica for scalable, environmentally friendly radiative cooling coatings. Ultimately, this work contributes to the development of next-generation inorganic cooling materials capable of reducing building energy demand while offering long-term stability and minimal environmental impact.

2. MATERIALS AND METHODS

2.1 Materials

The precursor material used in this study was a high-reactivity metakaolin, selected for its high amorphous content and consistent purity, properties known to facilitate effective geopolymerization under ambient curing. The alkaline activator solution consisted of a mixture of sodium hydroxide and sodium silicate, prepared freshly for each batch to ensure stable dissolution conditions and avoid premature gelation of silicate species. Biogenic silica nanoparticles, with an average particle size of 20–30 nm, derived from diatomaceous biosludge, were used as the baseline nanofiller. The biosludge served as a sustainable silica source rich in amorphous diatom frustules, enabling the production of highly reactive biogenic nanosilica suitable for geopolymer modification. Due to their high surface energy and associated tendency to agglomerate, a portion of the SiO_2 nanoparticles underwent surface modification using APTES, a silane coupling agent widely applied to enhance nanoparticle compatibility in aqueous or alkaline media. Ethanol and deionized water were used as solvents in the functionalization process. All raw materials were stored in sealed containers to minimize moisture adsorption and chemical degradation. Their chemical and physical properties were verified prior to use to ensure consistency with standard specifications (Table 1).

2.2 Synthesis of Biogenic SiO_2 Nanoparticles from Diatomaceous Biosludge

Diatomaceous biosludge was collected from the secondary sedimentation unit of a municipal wastewater treatment facility located in South India. This biosludge is predominantly composed of diatom frustules, which consist of amorphous biogenic silica formed through biological mineralization processes. The collected biosludge was first oven-dried at 105 °C for 24 h to remove free moisture and then mechanically ground to obtain a uniform powder. To eliminate residual organic matter while preserving the amorphous silica framework, the dried biosludge was subjected to controlled calcination at 600 °C for 3 h in a muffle furnace. This temperature was selected to ensure complete decomposition of organic residues without inducing

crystallization of the biogenic silica. The calcined material was subsequently dispersed in 2 M NaOH solution and heated at 90 °C under continuous stirring for 2 h to promote alkaline dissolution of silica species. The resulting sodium silicate-rich solution was filtered to remove insoluble mineral impurities. Biogenic silica was precipitated by the slow, dropwise addition of dilute hydrochloric acid under constant stirring until a neutral pH (≈7) was achieved. The precipitate was aged for 12 h to ensure complete condensation of silanol groups and then washed repeatedly with deionized water to remove residual sodium and chloride ions. The washed silica gel was dried at 80 °C for 24 h and lightly ground. To obtain nanoscale biogenic SiO_2, the dried powder was subjected to high-energy ball milling followed by ultrasonication in deionized water. This combined top-down approach produced biogenic silica nanoparticles with an average particle size of 20–30 nm and a predominantly amorphous structure. The resulting biogenic nanosilica exhibited a high density of surface silanol (–Si–OH) groups, making it particularly suitable for subsequent silane functionalization and effective participation in geopolymer gel formation. The overall silica recovery yield from the biosludge was approximately 65–70%, indicating the feasibility of scalable silica extraction from wastewater-derived diatomaceous residues.

2.3 Functionalization of SiO_2 with APTES

Functionalized silica nanoparticles were prepared through a silanization route involving hydrolysis and condensation reactions. The process began by dispersing biogenic SiO_2 nanoparticles derived from diatomaceous biosludge in a 70:30 ethanol–water mixture, followed by ultrasonic agitation to reduce soft agglomerates. APTES was hydrolyzed separately in the same solvent system under mildly acidic conditions (pH ≈ 4.5), a requirement for the activation of ethoxy groups. The hydrolyzed silane solution was then added dropwise to the silica dispersion under continuous stirring, allowing the APTES molecules to form covalent Si–O–Si bonds with surface hydroxyl groups on the nanoparticles.

The suspension was stirred for 2 h and subsequently heated to promote condensation. The modified nanoparticles were recovered by centrifugation, washed with ethanol to remove unreacted silane, and dried at 60 °C. The dried powder was lightly ground to maintain a uniform particle size distribution. Fig. 1 illustrates the synthesis of silica nanoparticles from diatomaceous biosludge. FTIR spectroscopy later confirmed successful grafting by the presence of N–H bending and C–H stretching vibrations associated with the APTES functional groups. The functionalized nanoparticles were expected to exhibit improved dispersion in the geopolymer slurry, reduced agglomeration, and enhanced compatibility with the aluminosilicate gel. The high density of surface silanol groups inherent to biogenic SiO_2 significantly enhanced the efficiency of APTES grafting compared to conventional synthetic silica. This resulted in improved steric stabilization, reduced nanoparticle agglomeration, and stronger interfacial compatibility with the geopolymer matrix. The functionalized biogenic nanosilica was therefore expected to promote more uniform gel formation and superior structure–property synergy in the resulting geopolymer coatings.

2.4 Preparation of Geopolymer Coatings

Three geopolymer systems were synthesized for comparative evaluation: a plain geopolymer (serving as the control group), a geopolymer containing unfunctionalized biogenic SiO_2 nanoparticles derived from diatomaceous biosludge, and a geopolymer incorporating APTES-functionalized biogenic SiO_2 nanoparticles. For all systems, the alkaline activator was prepared by dissolving NaOH pellets in deionized water and cooling the solution to room temperature before blending with sodium silicate (Table 2). This controlled preparation minimized temperature-driven reaction variability.

Table 1. Chemical and physical properties of raw materials

Material	Chemical Composition / Functional Groups	Physical Properties	Remarks
Metakaolin	SiO_2: 52–55%; Al_2O_3: 42–45%; minor Fe_2O_3, TiO_2	Median particle size: 5–8 µm; high amorphous phase	Geopolymer precursor
Biogenic SiO_2 nanoparticles (biosludge-derived)	Amorphous SiO_2 from diatom frustules	Particle size: 20–30 nm; irregular/frustule-derived morphology; BET surface area: 140–190 m^2/g	Waste-derived, highly reactive silica source
APTES-functionalized SiO_2 nanoparticles	Si–O–Si backbone; $–NH_2$ and $–CH_2–CH_2–CH_2–$ groups from APTES	Particle size: 25–35 nm; enhanced dispersibility; BET: 130–180 m^2/g	Better compatibility with the geopolymer matrix
NaOH pellets	≥98% NaOH	Solid pellets	Used for alkali activation
Sodium silicate solution	SiO_2/Na_2O ≈ 2.0–2.5; 35–40% solids	Viscous alkaline solution	Provides reactive silica
Ethanol	≥99.5% purity	Organic solvent	Used in SiO_2 functionalization
APTES	$C_9H_{23}NO_3Si$	Density ≈ 1.0 g/cm^3	Silane coupling agent

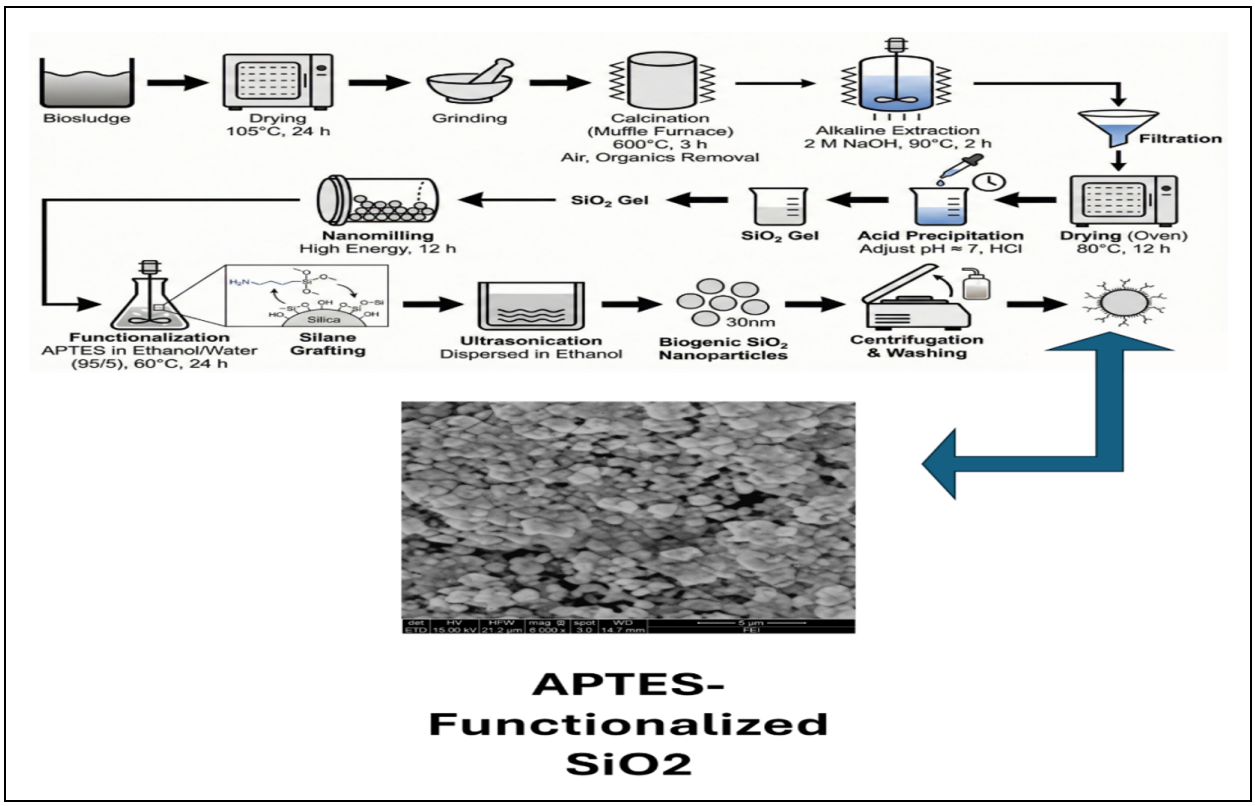


Fig. 1: Synthesis of diatomaceous sludge-derived, APTES-functionalized SiO_2

Table 2. Experimental groups

Component	Plain Geopolymer	Nano-SiO_2 Geopolymer	APTES-SiO_2 Geopolymer	Unit
Metakaolin (MK)	100	100	100	g
Sodium hydroxide solution	30	30	30	g per 100 g MK
Sodium silicate solution	40	40	40	g per 100 g MK
Additional water	Adjusted for workable slurry	Adjusted for workable slurry	Adjusted for workable slurry	g
Pristine SiO_2 nanoparticles	–	1.0	–	g per 100 g MK (wt.%)
APTES-functionalized SiO_2 nanoparticles	–	–	1.0	g per 100 g MK (wt.%)
Liquid-to-solid ratio (L/S)	0.45	0.45	0.45	–
Target coating thickness	500 ± 50	500 ± 50	500 ± 50	µm

The geopolymer slurry was produced by gradually blending metakaolin with the activator under mechanical mixing until a uniform paste developed. For nanoparticle-modified samples, either pristine or APTES-functionalized SiO_2 was first dispersed in water using ultrasonication for approximately 10 min to minimize aggregation. The resulting dispersion was introduced into the geopolymer slurry and mixed thoroughly to ensure homogeneity. This procedure was especially important for the APTES-SiO_2 system, in which enhanced surface compatibility was expected to result in more uniform distribution and improved interaction with the geopolymer matrix. A fixed nanoparticle loading of 1.0 wt.% was selected based on preliminary optimization trials, which indicated that this concentration provides an optimal balance between maximizing gel crosslinking and avoiding excessive agglomeration at higher dosages. The slurries were applied onto fiber-cement board substrates using a controlled draw-down coating technique to achieve a thickness of approximately 500 ± 50 µm. Coated specimens were left to cure at 25 ± 2 °C and approximately 60% relative humidity for seven days. This curing regime allowed sufficient dissolution of metakaolin particles and polycondensation of silico-aluminate species, leading to the formation of the geopolymer gel network. Each coating was visually examined to confirm uniformity, absence of defects, and adequate adhesion to the substrate.

2.5 Characterization Methods

2.5.1 Solar Reflectance Measurement

The solar reflectance properties of the coating systems were evaluated using a UV–Vis–NIR spectrophotometer equipped with an integrating sphere accessory. The instrument used was a PerkinElmer Lambda 950 model. Measurements were carried out over a broad wavelength range from 250 nm to 2500 nm, covering the ultraviolet (UV), visible (Vis), and near-infrared (NIR) regions of the electromagnetic spectrum. The integrating sphere facilitated the collection of diffusely reflected light from the coated surfaces, enabling an accurate determination of the total reflectance. This test aimed to quantify the coatings' ability to reflect incoming solar radiation, which directly impacts their capacity to reduce surface heating and improve energy efficiency in building applications. Higher solar reflectance values are desirable for cool roofing and reflective coatings, as they contribute to lowering ambient temperatures and reducing the urban heat island effect.

2.5.2 Infrared Emissivity Measurement

Infrared emissivity of the coatings was measured using an FTIR spectrometer (Bruker Vertex 70). The analysis focused on the mid-infrared (mid-IR) region, spanning from 6 to 20 μm, which is critical for thermal radiation emission. Special attention was given to the atmospheric window between 8 and 13 μm, where the Earth's atmosphere is most transparent, allowing effective radiative heat dissipation. The FTIR spectrometer was equipped with a mid-IR detector and a sample holder that allowed precise measurement of the emissivity of the coating surfaces at controlled temperatures. The data obtained provided insight into the thermal radiative properties of the coatings, which influence their ability to emit heat efficiently and contribute to passive cooling strategies in building design.

2.5.3 Structural and Phase Composition Analysis

XRD analysis was performed using a Bruker D8 Advance X-ray diffractometer. The equipment utilized Cu Kα radiation (wavelength of 1.5406 Å) and a theta-theta (θ–2θ) scanning configuration. The scans covered a 2θ range typically from 5° to 80°, with a step size of 0.02° and a counting time sufficient to obtain clear diffraction peaks. The primary goal was to examine the phase composition and structural features of the coatings. The presence of a broad amorphous hump around 20°–35° in 2θ was identified as an indicator of geopolymer gel formation, which is essential for the binder's structural integrity. Any shifts, peak broadening, or changes in intensity were analyzed to assess the influence of nanoparticle incorporation, particularly functionalized silica, on the crystalline and amorphous phases within the geopolymer matrix.

2.5.4 Chemical Bonding Characterization

Chemical bonding and molecular structure within the coatings were analyzed using FTIR spectroscopy. The instrument used was a Shimadzu IRAffinity-1S spectrometer, equipped with an attenuated total reflectance (ATR) accessory. Spectral data were collected in the range of 4000 to 400 cm^{-1}, focusing on the characteristic vibrational modes of the chemical groups present. The analysis aimed to identify Si–O–T (T = Si or Al) vibrations, hydroxyl (OH) groups, and specific signatures associated with APTES functionalization. These spectral features provided detailed insights into the chemical bonding environment, the degree of silanization, and the interactions between nanoparticles and the geopolymer matrix, which influence the coating's chemical stability and adhesion properties.

2.5.5 Microstructural Examination

The microstructure of the coatings was examined using a scanning electron microscope (FEI Quanta 650). Prior to imaging, samples were prepared by sputter-coating with a thin layer of gold or platinum to prevent charging. SEM imaging was performed at accelerating voltages typically ranging from 5 to 20 kV. The high-resolution images provided detailed information about the surface morphology, nanoparticle distribution, pore size, and distribution, and the overall structural integrity of the coatings. This microstructural analysis was crucial for understanding how nanoparticle incorporation, especially functionalized silica, affected the coating's physical appearance, uniformity, and potential defect formation.

2.5.6 Thermal Behavior Analysis

Thermal stability and decomposition characteristics of the coatings were evaluated using thermogravimetric analysis (TGA) and differential thermal analysis (DTA), conducted using a NETZSCH STA 449 F3 Jupiter or similar instrument. The measurements were carried out from ambient temperature (around 25 °C) up to 1000 °C at a heating rate of 10 °C per min under a flowing inert gas such as nitrogen or air. TGA measured the mass loss associated with dehydration, dehydroxylation, and structural decomposition, while DTA detected endothermic or exothermic transitions related to phase changes or chemical reactions. The combined data enabled a comprehensive comparison of the thermal stability, decomposition stages, and residual char content across the three different coating formulations.

2.5.7 Mechanical Property Evaluation

The mechanical performance of the geopolymer coatings was assessed through a series of standardized tests. Compressive strength tests were conducted on cubic or cylindrical specimens of the bulk geopolymer

using a universal testing machine (UTM), Instron 5967, following ASTM C109 standards. The samples were tested at a controlled rate of loading until failure, providing data on the compressive strength, which reflects the structural integrity of the binder. In addition, hardness was measured using a Vickers hardness tester, and adhesion tests, such as pull-off or cross-hatch adhesion tests, were conducted using a DioTest adhesion tester. These tests evaluated the coating's ability to withstand mechanical stresses and adhere firmly to substrates. The results provided critical insights into how the incorporation of functionalized silica nanoparticles influenced the durability, structural robustness, and long-term performance of the coatings under mechanical loading conditions. All mechanical evaluations were performed in triplicate to account for material variability, and results are reported as the mean ± standard deviation.

2.6 Field Radiative Cooling Performance Evaluation

The radiative cooling performance of the geopolymer coatings was evaluated under real outdoor conditions to determine their ability to achieve sub-ambient surface temperatures during daytime exposure. Coated and uncoated fiber-cement boards were placed on an unobstructed rooftop area with direct access to sunlight to avoid shading effects or reflective interference from nearby structures. Each sample was mounted within a thermally insulated frame fabricated from polystyrene foam and lined internally with aluminum foil. This configuration minimized heat exchange with the supporting surface and ensured that the measured temperatures predominantly reflected the radiative behavior of the coatings rather than substrate conduction effects. Surface temperatures were monitored continuously using Type-K thermocouples positioned at the interface between the coating layer and the cement board substrate. The thermocouples were secured using a high-temperature adhesive tape to maintain consistent thermal contact throughout the measurement period. Data were recorded at one-minute intervals using a multi-channel digital data logger with an accuracy of ±0.1 °C. Prior to installation, all thermocouples were calibrated using an ice-water bath and a dry-block calibrator to ensure consistency across measurement channels. To capture the environmental boundary conditions that govern radiative cooling behavior, a portable automatic weather station was installed adjacent to the test samples. The station continuously monitored ambient air temperature, relative humidity, solar irradiance, and wind speed, as these parameters influence both convective heat losses and the radiative exchange between the coating surface and the sky dome. All environmental data were synchronized with thermal measurements to allow for accurate correlation between coating performance and atmospheric conditions. Tests were conducted over a full 24-hour cycle to capture diurnal variations in solar exposure and nighttime infrared heat loss. Daytime performance was evaluated by examining the ability of the coatings to maintain surface temperatures below those of the uncoated sample and below the ambient air. Night-time measurements provided additional insight into the coatings' emissivity-driven heat rejection capabilities, although the primary focus remained on daytime sub-ambient cooling. The plain geopolymer coating, nano-SiO_2 geopolymer coating, and APTES-functionalized SiO_2 geopolymer coating were evaluated simultaneously under identical outdoor conditions to ensure direct comparability.

3. RESULTS AND DISCUSSION

3.1 XRD Analysis

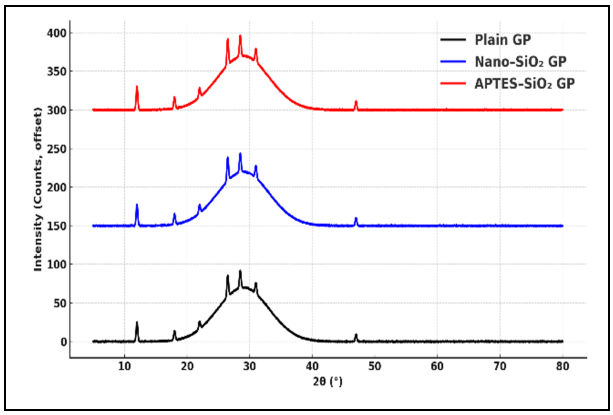


Fig. 2: XRD patterns of geopolymer systems

Fig. 2 shows the XRD patterns of the plain geopolymer (GP), nano-SiO_2-modified GP, and APTES-functionalized SiO_2 GP, plotted with vertical offsets for clarity. All three formulations show the characteristic amorphous aluminosilicate hump centred around 27–33°, which is typically associated with the disordered Q^3–Q^4 silicate network of geopolymer gels. The plain geopolymer displays a broad, low-intensity envelope, consistent with incomplete dissolution of metakaolin plates and the formation of a partially polymerized sodium aluminosilicate hydrate gel. With the incorporation of unmodified nano-SiO_2, a marked increase in the hump intensity is observed, indicating a higher degree of silicate re-polymerization and greater crosslink density within the gel framework. This observation agrees with previous studies reporting that nanosilica accelerates monomer formation, enhances polycondensation, and promotes early-stage nucleation of N-A-S-H gel domains. The visible increase in scattering intensity between 25° and 35° supports the hypothesis that nanosilica participates both as a reactive silica source and as a surface for heterogeneous nucleation of aluminosilicate species. The APTES-functionalized SiO_2 geopolymer exhibits the strongest and sharpest amorphous hump among the three matrices. This suggests more efficient integration of the

functionalized nanoparticles into the geopolymer network, likely due to their enhanced interfacial bonding capability. The primary amine groups of APTES are known to interact with dissolved aluminate and silicate oligomers, improving their dispersion stability and facilitating more extensive gel formation (Dhaffouli *et al.* 2024). This improved compatibility is reflected in the increased intensity and reduced breadth of the amorphous hump. In addition to the amorphous region, distinct crystalline reflections appear at approximately 12°, 18°, 22°, 26°, 28.5°, 31°, and 47°. These peaks correspond to unreacted metakaolin phases (Si–O–Al), minor aluminate phases, and quartz impurities (N'cho *et al.* 2023). Their relative intensity increases slightly in the modified systems, particularly in APTES–SiO_2 GP, likely due to improved nanoparticle dispersion enhancing X-ray scattering rather than increased crystallinity. The absence of new crystalline phases confirms that functionalization and nanoparticle incorporation do not alter the fundamental amorphous geopolymer matrix but instead modify its polymerization state. The enhanced amorphous character observed in the biogenic SiO_2-modified systems can be further attributed to the inherently disordered nature of diatom-derived silica. Biogenic silica lacks long-range crystalline order, which enhances its reactivity in alkaline media and facilitates more efficient incorporation into the geopolymer gel network. This characteristic distinguishes waste-derived nanosilica from conventional synthetic counterparts and contributes to the observed increase in polymerization extent. Collectively, the XRD results indicate a clear trend: Plain GP < Nano-SiO_2 GP < APTES-SiO_2 GP in terms of structural ordering, polymerization extent, and gel phase development. These findings establish the structural foundation for the performance enhancements discussed in subsequent sections.

3.2 FTIR Spectral Analysis

Fig. 3 shows the FTIR spectra of the three geopolymer systems in the range of 4000–400 cm^{-1}, revealing distinct chemical signatures associated with gel formation and nanoparticle incorporation. All samples display a dominant asymmetric stretching band of Si–O–T (T = Si or Al) centered between 1030 and 1080 cm^{-1}, characteristic of geopolymer gels. Notably, the position of this band shifts systematically across the formulations: the plain geopolymer exhibits a peak near ~1070 cm^{-1}, which shifts to ~1060 cm^{-1} in the nano-SiO_2 GP and further to ~1050 cm^{-1} in the APTES-functionalized system. This progressive redshift reflects increasing polymerization and a growing presence of Si–O–Si linkages relative to Si–O–Al bonds. The incorporation of nano-SiO_2 provides additional reactive silica, promoting more complete condensation of silicate species. For the APTES–SiO_2 GP, the larger shift suggests even greater structural reorganization, consistent with enhanced nanoparticle–matrix compatibility facilitated by APTES-derived silane coupling reactions. All spectra exhibit O–H stretching vibrations around 3400 cm^{-1} and H–O–H bending near 1640 cm^{-1}, corresponding to physically absorbed and interlayer water (Zidi *et al.* 2021). The intensity of these bands decreases slightly for the nano-SiO_2 and APTES–SiO_2 samples, supporting the conclusion that nanoparticle addition densifies the geopolymer matrix and reduces free water content. Such trends correlate with the densification observed in SEM analysis. Characteristic metakaolin Al–OH bending modes at ~915 cm^{-1} appear faintly in the plain geopolymer but nearly disappear in nanoparticle-modified matrices, suggesting more complete dissolution of the precursor and stronger gel formation (Ivanovic *et al*. 2020).

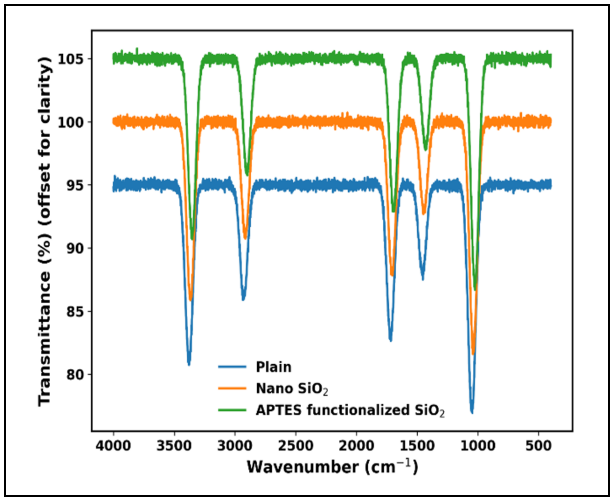


Fig. 3: FTIR spectra of geopolymer systems

Additional small features near 1450–1500 cm^{-1} and 2850–2950 cm^{-1} can be associated with surface-adsorbed carbonate species and C–H stretching vibrations, respectively. A unique feature of the APTES–SiO_2 modified geopolymer is the slight broadening around 1550–1580 cm^{-1}, attributable to N–H bending from the amine groups of APTES. Although subtle, this band confirms the chemical retention of grafted APTES on nanoparticle surfaces after geopolymerization. Overall, FTIR results corroborate XRD findings, showing that APTES functionalization yields the most chemically evolved and polymerized geopolymer structure. These spectral signatures confirm the enhanced role of functionalized nanoparticles in reinforcing the geopolymer network at the molecular scale.

3.3 Microstructural Characterization

SEM was employed to examine the surface morphology and dispersion characteristics of pristine SiO_2 nanoparticles and APTES-functionalized SiO_2. The SEM micrographs of the unmodified SiO_2 nanoparticles in Fig. 4a reveal predominantly spherical particles with relatively smooth surfaces and a narrow size distribution. However, due to the high surface energy and strong van

der Waals attraction among particles, noticeable agglomeration is observed, forming irregular clusters. These aggregates are typical of nanosilica systems and can limit effective dispersion in matrices if not surface-modified. In contrast, the SEM images of APTES-functionalized SiO_2 nanoparticles (Fig. 4b) exhibit a slightly rougher surface texture, indicating the successful grafting of organosilane molecules onto the nanoparticle surface. The particles appear more uniformly dispersed with reduced agglomeration compared to the pristine SiO_2, suggesting that the introduction of aminopropyl functional groups improves interparticle repulsion and steric stabilization. The presence of a thin organic coating layer around the nanoparticles can also be inferred from the marginal increase in apparent particle size and the less compact clustering observed in the micrographs. Furthermore, the SiO_2-APTES nanoparticles display improved spatial separation and a more homogeneous distribution, which is advantageous for enhancing interfacial bonding when incorporated into composite or cementitious matrices. The modification effectively alters the surface chemistry without significantly changing the overall particle morphology, confirming that the functionalization process preserves the structural integrity of the silica nanoparticles while improving their dispersion behavior.

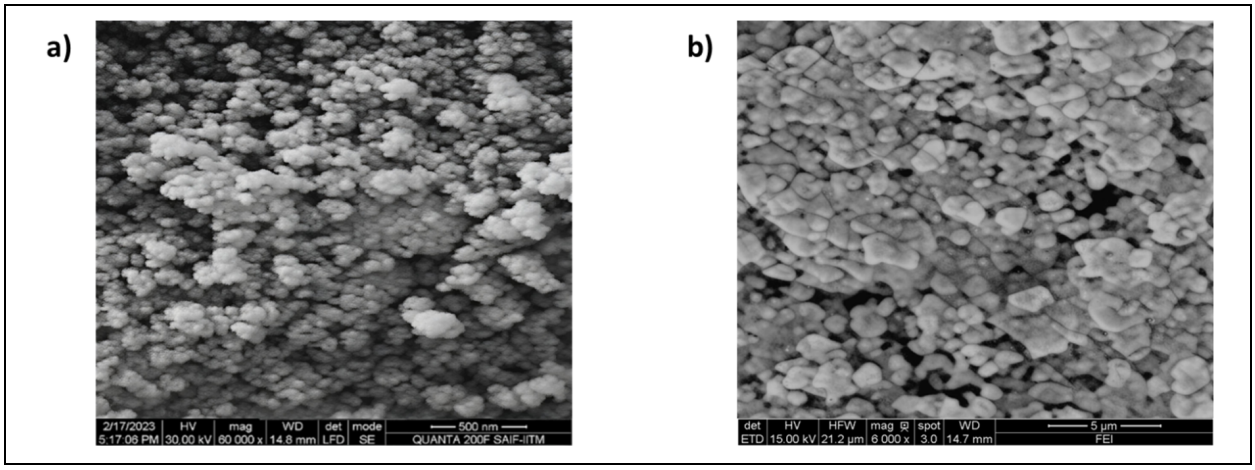


Fig. 4: (a) SEM micrographs of (a) pristine SiO_2 nanoparticles showing predominantly spherical morphology with smooth surfaces and noticeable agglomeration due to high surface energy and (b) APTES-functionalized SiO_2 nanoparticles exhibiting slightly roughened surfaces, reduced agglomeration, and improved particle dispersion, indicating successful surface modification

SEM and EDX analyses of the modified geopolymer coatings reveal pronounced microstructural transitions associated with nanosilica addition. The plain geopolymer exhibits a discontinuous matrix with angular metakaolin remnants, broad intergranular voids, and microcracks, indicating incomplete precursor dissolution (Naskar *et al.* 2016). In contrast, the nano-SiO_2 geopolymer reveals a substantially more consolidated network with smoother gel surfaces and narrower pore throats. This indicates that the high surface area of nanosilica accelerates silicate dissolution and provides abundant nucleation sites for secondary gel formation (Wen *et al.* 2020). The APTES-functionalized SiO_2 geopolymer demonstrates the most structurally advanced microarchitecture. SEM images show an exceptionally coherent gel matrix with minimal microcracking and near-total absence of unreacted metakaolin. The amine-functional silane suppresses nanoparticle agglomeration through steric stabilization and provides interfacial siloxane bridges (Si–O–Si) that chemically integrate the nanoparticles into the framework (Woźnica *et al.* 2023). This interfacial compatibilization enhances gel-phase cohesion and promotes a more uniform polymerization front, resulting in a highly homogeneous morphology. EDX results reinforce this interpretation.

The plain geopolymer displays a moderate Si/Al signature characteristic of poorly polymerized N–A–S–H gel. Nano-SiO_2 incorporation enriches the silica content, increasing the Si/Al atomic ratio as expected from enhanced gel crosslinking. The APTES–SiO_2 system exhibits an even higher Si abundance, accompanied by distinct nitrogen and carbon peaks at 0.39 and 0.27 keV, respectively—direct evidence of the chemically retained organosilane layer. The presence of nitrogen confirms that APTES participates in interfacial reactions rather than being volatilized or leached during synthesis, strongly suggesting covalent anchoring of the functionalized nanoparticles within the polymeric framework. This interfacial chemistry provides a structural explanation for the observed improvements in compressive strength, thermal stability, and radiative optical performance. The hierarchical morphology inherited from diatomaceous silica also plays a significant role in microstructural refinement. The frustule-derived surface texture of biogenic SiO_2 introduces multiscale interfacial features that promote gel anchoring and suppress localized stress concentration. This effect is particularly pronounced in the APTES-functionalized system, where chemical bonding and physical interlocking operate synergistically to produce

an exceptionally compact and defect-free geopolymer microstructure. Collectively, the SEM/EDX results establish a clear structure–property relationship: nanosilica enhances geopolymerization through nucleation and reactive silica supply, while APTES introduces molecular-level interfacial compatibility that maximizes gel continuity and suppresses mesoscale defects. These microstructural enhancements form the mechanistic foundation for the superior multifunctional performance of the APTES–SiO_2 geopolymer coating observed across mechanical, thermogravimetric, and optical characterizations.

3.4 TGA

Fig. 6 presents the thermogravimetric behaviour of the plain geopolymer (GP), nano-SiO_2 GP, and APTES–SiO_2 GP from 30 °C to 900 °C. All samples exhibit a continuous mass loss characteristic of aluminosilicate geopolymers, but with clear differences in the rate and extent of degradation. These variations directly reflect the influence of nanoparticle dispersion, interfacial chemistry, and the degree of aluminosilicate gel polymerization. The plain geopolymer shows the highest cumulative mass loss, decreasing to approximately 47 wt.% at 900 °C. The initial region (30–150 °C) corresponds primarily to the evaporation of physically bound water trapped within interlayer sites and mesopores, a behaviour consistent with earlier geopolymer studies (Ngouloure *et al.* 2022). This is followed by a gradual but steady mass loss between 150 and 400 °C, attributable to the removal of chemisorbed water and dehydroxylation of residual metakaolin phases. The more pronounced weight reduction in the plain sample indicates incomplete geopolymerization and a more porous gel structure, which retains greater

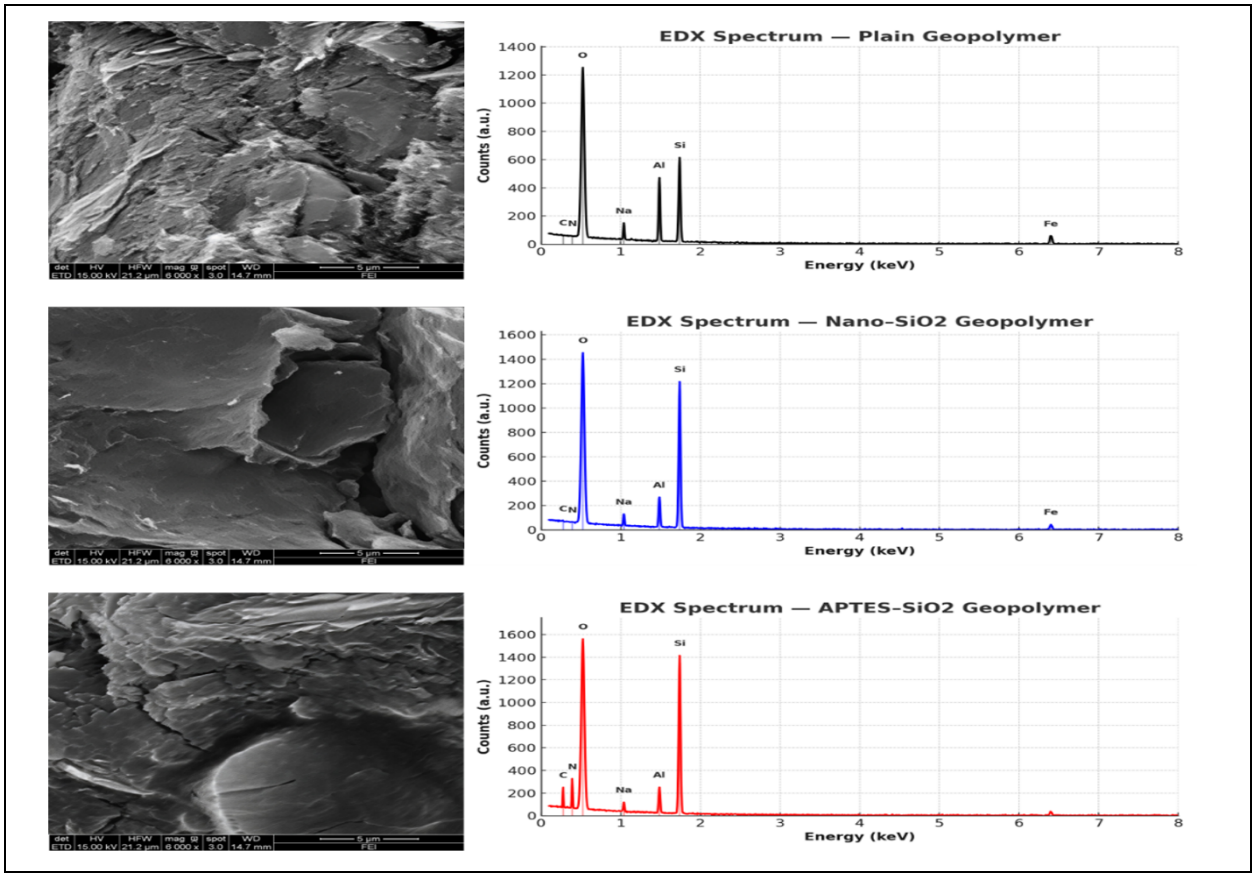


Fig. 5: SEM/EDX analyses of (a) plain geopolymer, (b) nano-SiO_2 geopolymer, and (c) APTES-functionalized nano-SiO_2 geopolymer

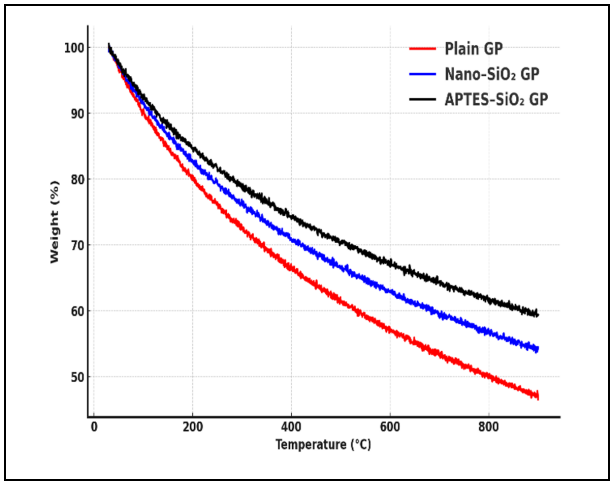


Fig. 6: TGA of geopolymer systems

moisture and exhibits weaker binding forces. The incorporation of nano-SiO_2 significantly improves thermal stability. The nano-SiO_2 GP retains approximately 55 wt.% of its mass at 900 °C, an 8% improvement over the plain GP. This enhancement is linked to nanosilica acting as a reactive silicate donor, which increases the Si/Al ratio and promotes the formation of more cross-linked siloxane networks (Qu *et al*. 2024). The reduced slope of the TGA curve from 200–500 °C suggests reduced structural water and fewer hydroxyl groups, consistent with a denser, more evolved geopolymer gel. The APTES-functionalized SiO_2 GP demonstrates the highest thermal resistance, retaining ~60 wt.% mass at 900 °C. The shift in thermal profile is attributed to two synergistic effects: (1) enhanced nanoparticle dispersion due to the amine-functional silane layer, which minimizes agglomeration and maximizes their participation in gel formation; and (2) interfacial covalent bonding between APTES and aluminosilicate species, which strengthens the molecular network.

The slower mass-loss rate across the full temperature range indicates not only reduced water content but also a more thermally stable binding environment, consistent with improved polymerization observed in XRD and FTIR analyses. Across all samples, no abrupt weight losses are detected above 500 °C, confirming the absence of carbon-containing additives or thermally unstable organic phases. The smooth decay is characteristic of geopolymer matrices undergoing continued dehydroxylation and structural rearrangement at elevated temperatures (Tran and Ngo, 2025). The ordering of thermal stability follows the trend: APTES–SiO_2 GP > nano-SiO_2 GP > Plain GP. This trend strongly supports the hypothesis that surface-functionalized nanoparticles contribute to a more cohesive, chemically integrated geopolymer network. These improvements in thermal robustness are expected to translate into enhanced durability and service life in high-temperature or cyclic heat-exposure environments.

3.5 Optical Properties

3.5.1 UV–Vis–NIR Reflectance Behaviour

The UV–Vis–NIR reflectance spectra in Fig. 7 reveal distinct differences in solar optical behaviour among the three geopolymer systems. The plain geopolymer exhibits the lowest reflectance across the full wavelength range, remaining between 5% and 11%, which is consistent with dense aluminosilicate matrices lacking effective scattering centers (Ibrahim *et al*. 2025). The limited porosity and absence of high-refractive-index inclusions lead to strong absorption and internal damping of incident photons, a behaviour similarly reported for unmodified metakaolin-based geopolymers

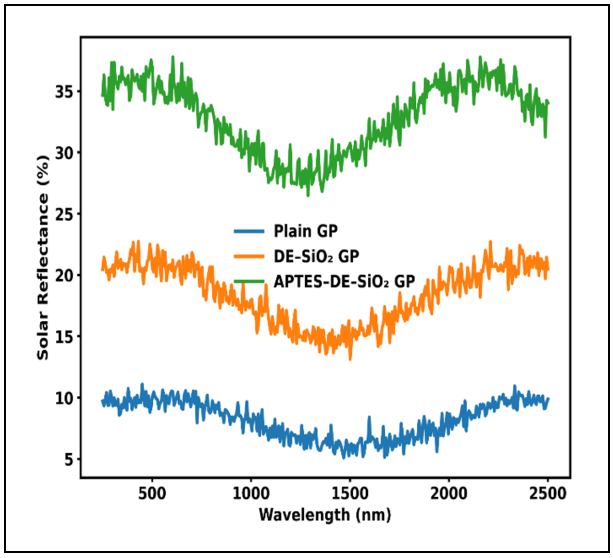


Fig. 7: Solar reflectance spectra of geopolymer systems

(Mahrous *et al.* 2024). With the addition of nano-SiO_2, broadband reflectance increases substantially, reaching values between 14% and 22%. This enhancement is attributed to additional dielectric contrast and increased internal interfaces formed by uniformly dispersed nanospheres, enabling Mie scattering that reduces photon penetration depth and mitigates near-infrared absorption losses. The suppression of the reflectance trough around 1000–1300 nm further suggests reduced vibrational absorption associated with the aluminosilicate framework, likely due to the refinement of gel-phase microstructure (Rees *et al.* 2007). The APTES-functionalized SiO_2 geopolymer demonstrates the highest reflectance, reaching up to 36% across the measured spectrum. Functionalization improves nanoparticle dispersion and minimizes agglomeration, enabling more uniform incorporation into the geopolymer network and promoting the development of hierarchical porosity capable of multiple scattering (Yang *et al*. 2025). This behaviour, reflected in the broad M-shaped reflectance profile, corresponds to enhanced spectral selectivity and superior solar management

performance, consistent with similar observations in functionalized nanoparticle–polymer cooling systems (Bai *et al.* 2017). Overall, the reflectance results indicate that functionalized nanofillers provide a significant advantage in reducing solar heat gain and optimizing the coating for radiative cooling applications. In addition to improved dispersion, the superior reflectance performance of the APTES-functionalized biogenic SiO_2 geopolymer is influenced by the unique light-scattering behavior of diatom-derived silica. The residual nanoscale structural irregularities originating from diatom frustules enhance multiple internal scattering pathways, contributing to broadband solar reflectance enhancement beyond that achievable with purely synthetic spherical silica nanoparticles.

3.5.2 Infrared Emissivity Characteristics

Fig. 8 illustrates the mid-infrared emissivity characteristics of the plain, nano-SiO_2, and APTES–SiO_2 geopolymer coatings. All samples exhibit high emissivity outside the characteristic Si–O vibrational absorption bands, approaching values close to unity, which is typical of aluminosilicate structures with strong phonon activity and broad IR absorption tails (Giacomazzi *et al.* 2023). The plain geopolymer shows the deepest emissivity minima, dropping to 0.82–0.84 in regions associated with Si–O–T stretching bands near 1050–1100 cm^{-1} and Si–O bending modes around 450–500 cm^{-1}, reflecting structural heterogeneity and incomplete geopolymerization. Nano-SiO_2 addition results in shallower emissivity dips, rising to 0.85–0.87, indicative of enhanced crosslinking and fewer radiatively inactive domains within the gel framework.

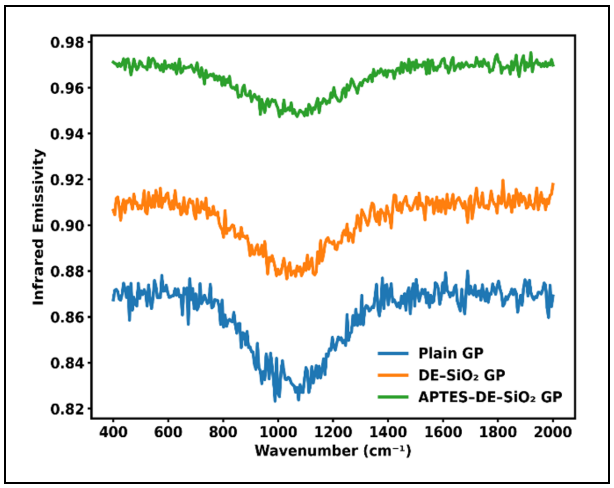


Fig. 8: Infrared emissivity spectra of geopolymer systems

This correlates well with XRD and FTIR evidence showing improved polymerization and increased Si–O–Si linkage formation. The APTES-functionalized SiO_2 geopolymer displays the most favourable IR behaviour, maintaining emissivity values near 0.98–1.00 outside the vibrational troughs and showing only moderately depressed minima (0.88–0.90). These improvements suggest that silane functionalization enhances interfacial bonding between the nanoparticles and the gel matrix, promoting more efficient phonon transport and reducing vibrational disorder, which are critical for sustaining high IR output (Niranjana *et al.* 2025). The overall pattern indicates that functionalized nanoparticles not only improve structural integrity but also amplify thermal radiation efficiency, positioning the APTES–SiO_2 system as superior for mid-IR radiative cooling functions.

3.5.3 Implications for Radiative Cooling Performance

The combined reflectance and emissivity data demonstrate a coherent optical enhancement that directly influences the radiative cooling capability of the coatings. High broadband solar reflectance significantly reduces heat absorption during daytime exposure, while strong mid-infrared emissivity ensures effective thermal radiation through the atmospheric transparency window—a dual requirement for sub-ambient cooling performance (Meng *et al.* 2020). The plain geopolymer shows limited potential for daytime cooling due to its low reflectance and pronounced emissivity minima, which restrict its ability to reject solar radiation and emit stored heat. Conversely, the nano-SiO_2-modified geopolymer presents a more favourable profile by reducing absorption losses and improving network homogeneity, thereby providing a measurable enhancement in radiative cooling efficiency. The APTES-functionalized SiO_2 geopolymer performs optimally, with the highest reflectance and near-ideal emissivity behaviour. This combination implies that the functionalized coating can maintain lower surface temperatures under realistic environmental conditions, consistent with the cooling effects reported in advanced inorganic and hybrid radiative coatings (Feng *et al.* 2023). The optical results therefore reinforce that functionalized nanoparticles offer a strategic pathway for engineering geopolymer matrices with superior radiative cooling potential, enabling their deployment as sustainable alternatives to polymer-based coatings.

3.6 Mechanical Properties

The compressive strength results presented in Fig. 9 reveal a clear and systematic enhancement in mechanical performance with the incorporation of nanosilica and APTES-functionalized nanosilica into the geopolymer matrix. The plain geopolymer exhibited a compressive strength of 18.5 MPa, which is consistent with values typically observed for metakaolin-based geopolymers synthesized without supplementary reactive silica or coupling additives (Bezerra *et al.* 2023). The relatively modest strength can be attributed to incomplete dissolution of the aluminosilicate precursor, limited Si–O–Si crosslink density, and the presence of microvoids generated during the polycondensation

process. These structural limitations reduce load-bearing continuity and produce localized stress concentrations that facilitate crack initiation and early failure. In contrast, the nano-SiO_2-modified geopolymer achieved a significantly higher strength of 26.8 MPa, reflecting the beneficial role of nanosilica as a highly reactive pozzolanic additive. The nanoparticles act as nucleation sites for gel formation, consuming free alkalis and dissolved silicate species to produce a denser, more crosslinked network characterized by increased Si–O–Si polymerization (Liu *et al.* 2017). The improved packing efficiency and refined microstructure reduce capillary porosity and enhance stress-transfer efficiency, explaining the ~45% increase in mechanical performance relative to the plain matrix.

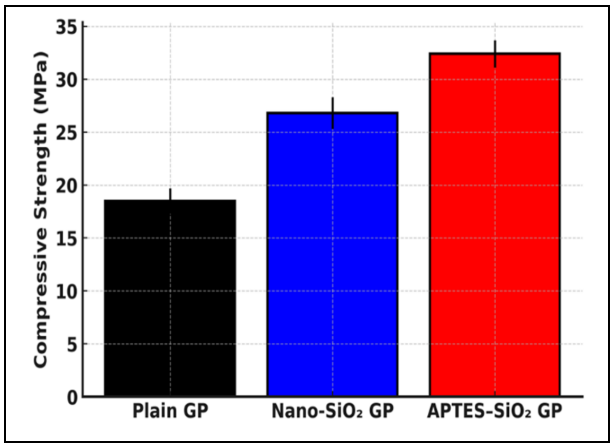


Fig. 9: Mechanical properties of geopolymer coatings

The highest compressive strength was obtained for the APTES–SiO_2-modified geopolymer, which reached 32.4 MPa. This substantial enhancement highlights the effectiveness of functionalization in improving nanoparticle dispersion and interfacial compatibility with the surrounding gel. The amine groups of APTES form covalent and hydrogen bonding interactions with aluminosilicate oligomers, producing a more seamless particle–matrix interface that inhibits nanoparticle agglomeration (Mousavi and Fini, 2020). This leads to a highly uniform gel network with fewer structural defects and reduced microcracking propensity, mirroring improvements reported in silane-functionalized nanocomposites (Sujitha *et al*. 2024). The resulting hierarchy—APTES–SiO_2 GP > Nano-SiO_2 GP > Plain GP—confirms that nanoparticle surface chemistry plays a decisive role not only in the geopolymerization kinetics but also in the mechanical integrity of the final composite.

3.7 Field Radiative Cooling Performance

Fig. 10 illustrates the 24-hour surface temperature profiles of the plain, nano-SiO_2, and APTES-SiO_2 geopolymer coatings under real outdoor exposure, compared against ambient temperature. The plain geopolymer displayed the poorest thermal performance, with surface temperatures rising to 36 °C at midday, approximately 4 °C above ambient. This behaviour stems from its low broadband reflectance and inadequate suppression of near-infrared absorption, resulting in significant solar heat gain (Jiang *et al.* 2022). The weak emissivity minima further limit the ability of the plain material to dissipate stored heat through longwave IR radiation, causing elevated temperatures throughout the diurnal cycle. To ensure the reliability of these measurements, environmental variability was continuously tracked. During the peak daytime testing period, average solar irradiance was approximately 850 ± 50 W/m², relative humidity fluctuated between 45–60%, and ambient wind speeds averaged 1.5 ± 0.5 m/s. Despite these dynamic boundary conditions, the cooling performance trends remained distinct. The nano-SiO_2 geopolymer demonstrated a moderate radiative cooling effect, maintaining surface temperatures consistently 0.5–1.0 °C below ambient during daytime. This improvement can be directly linked to the enhanced optical properties observed earlier: increased reflectance between 350–2500 nm and higher mid-IR emissivity relative to the plain matrix. These modifications reduce solar heat absorption and increase longwave radiative emission, yielding a measurable reduction in surface temperature. However, the extent of cooling remains limited by partial nanoparticle agglomeration and incomplete suppression of mid-IR absorption bands.

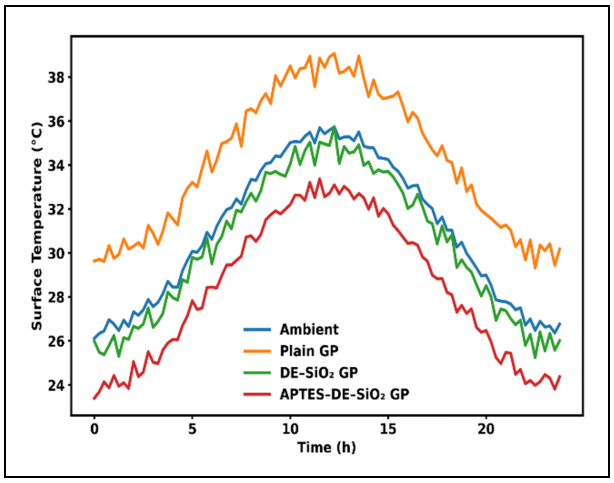


Fig. 10: Field radiative cooling performance of geopolymer coatings

The APTES–SiO_2-modified geopolymer exhibited the most pronounced cooling capability, achieving 2–3 °C sub-ambient temperatures at peak solar conditions, with a minimum of ~22 °C compared to the ambient 24 °C. This superior performance arises from the synergistic combination of the highest measured solar reflectance and near-unity infrared emissivity across much of the radiative window. The homogeneous dispersion of functionalized nanoparticles increases multiple scattering within the coating and introduces

additional phonon-active interfaces, enabling more efficient transmission of thermal radiation to the sky (Safdar *et al.* 2024). This behaviour aligns with reports on high-performance inorganic radiative cooling materials capable of passive sub-ambient cooling even under direct sunlight. The sharper cooling response during mid-day and faster night-time thermal dissipation validates the structural and optical improvements achieved through functionalization, confirming the APTES-SiO_2 geopolymer as the most promising candidate for real-world radiative cooling applications.

4. CONCLUSION

This study demonstrates that biogenic SiO_2 nanoparticles derived from diatomaceous biosludge serve as highly effective functional additives for geopolymer-based radiative cooling coatings. While plain geopolymers exhibited incomplete polymerization and insufficient solar reflectance, resulting in above-ambient surface temperatures, the incorporation of biogenic nanosilica refined the pore structure and improved structural crosslinking. The most significant enhancements occurred when biogenic nanosilica was surface-functionalized with APTES. This functionalization ensured uniform dispersion and robust interfacial bonding, yielding the highest compressive strength (32.4 MPa), enhanced broadband solar reflectance (~36%), and near-unity infrared emissivity. Consequently, the APTES-modified coating achieved consistent sub-ambient daytime cooling of 2–3 °C under direct sunlight. These findings establish that surface-functionalized, waste-derived biogenic silica provides a sustainable, scalable pathway for developing low-carbon, non-polymeric cooling infrastructure for hot climates. Future work could focus on evaluating long-term durability under cyclic weathering and UV exposure.

FUNDING

This research received no specific grant from any funding agency in the public, commercial, or not-for-profit sectors.

CONFLICTS OF INTEREST

The authors declare that there is no conflict of interest.

COPYRIGHT

This article is an open-access article distributed under the terms and conditions of the Creative Commons Attribution (CC BY) license (http://creativecommons.org/licenses/by/4.0/).

REFERENCES

Bai, Y., Li, Z., Cheng, B., Zhang, M. and Su, K., Higher UV-shielding ability and lower photocatalytic activity of TiO_2@SiO_2/APTES and its excellent performance in enhancing the photostability of poly (p-phenylene sulfide), *RSC Adv.,* 7(35), 21758–21767 (2017). https://doi.org/10.1039/C6RA28098F

Bezerra, B. P., Morelli, M. R. and Luz, A. P., Effect of reactive silica sources on the properties of Na-metakaolin-based geopolymer binder, *Constr. Build. Mater.,* 364, 129989 (2023). https://doi.org/10.1016/j.conbuildmat.2022.129989

Chetan, V., Nagaraj, K., Kulkarni, P. S., Modi, S. K. and Kempaiah, U. N., Review of passive cooling methods for buildings, *J. Phys.: Conf. Ser.,* 1473(1), 012054 (2020). https://doi.org/10.1088/1742-6596/1473/1/012054

Dhaffouli, A., Salazar, -C. P. A., Carinelli, S., Holzinger, M. and Barhoumi, H., Improved electrochemical sensor using functionalized silica nanoparticles (SiO2-APTES) for high selectivity detection of lead ions, *Mater. Chem. Phys*., 318, 129253 (2024). https://doi.org/10.1016/j.matchemphys.2024.129253

Feng, S., Yao, L., Feng, M., Cai, H., He, X., Bu, X., Huang, Y., Zhou, Y. and He, M., Superamphiphobic interface-enhanced inorganic coating for multi-environments tolerant and zero-energy building radiative cooling, *Chem. Eng. J.,* 475, 146191 (2023). https://doi.org/10.1016/j.cej.2023.146191

Gao, W. and Chen, Y., Emerging materials and strategies for passive daytime radiative cooling, *Small,* 19(18), 2206145 (2023). https://doi.org/10.1002/smll.202206145

Giacomazzi, L., Shcheblanov, N. S., Povarnitsyn, M. E., Li, Y., Mavrič, A., Zupančič, B., Grdadolnik, J. and Pasquarello, A., Infrared spectra in amorphous alumina: A combined ab initio and experimental study, *Phys. Rev. Mater.,* 7(4), 045604 (2023). https://doi.org/10.1103/PhysRevMaterials.7.045604

Griffith, M. J., Cooling, N. A., Vaughan, B., Elkington, D. C., Hart, A. S., Lyons, A. G., Quereshi, S., Belcher, W. J. and Dastoor, P. C., Combining printing, coating, and vacuum deposition on the roll-to-roll scale: A hybrid organic photovoltaics fabrication, *IEEE J. Sel. Top. Quantum Electron.,* 22(1), 112–125 (2015). https://doi.org/10.1109/JSTQE.2015.2487968

Hitchin, R., Primary Energy Factors and the primary energy intensity of delivered energy: An overview of possible calculation conventions, *Build. Serv. Eng. Res. Technol.,* 40(2), 198–219 (2019). https://doi.org/10.1177/0143624418799716

Hughes, B. R., Chaudhry, H. N. and Ghani, S. A., A review of sustainable cooling technologies in buildings, *Renewable Sustainable Energy Rev.,* 15(6), 3112–3120 (2011). https://doi.org/10.1016/j.rser.2011.03.032

Ibrahim, S., Fayad, A. M., El-Kheshen, A. A., Hamdy, Y. M., Ibrahim, M. M. and Marzouk, M. A., Characterization and optimization of amorphous alumina-doped silica thin layer material of low emissivity coating technology for energy-saving applications, *Energy Build.,* 341, 115836 (2025). https://doi.org/10.1016/j.enbuild.2025.115836

Ivanović, M., Kljajević, L. M., Gulicovski, J., Petković, M., Janković-Častvan, I., Bučevac, D. and Nenadović, S., The effect of the concentration of alkaline activator and aging time on the structure of metakaolin based geopolymer, *Sci. Sintering,* 52(2), 219–229 (2020). https://doi.org/10.2298/SOS2002219I

Jagajeevan, V. and Sivakumar, V. L., Silane-grafted g-C_3N_4 nanosheet enhanced air monitoring filters for PM2.5 capture and detection in urban environments, *Environ. Nanotechnol., Monit. Manage.,* 25, 101129 (2026). https://doi.org/10.1016/j.enmm.2026.101129

Jiang, L., Zhou, S., Yang, J., Wang, H., Yu, H., Chen, H., Zhao, Y., Yuan, X., Chu, W. and Li, H., Near-infrared light responsive TiO_2 for efficient solar energy utilization, *Adv. Funct. Mater.,* 32(12), 2108977 (2022). https://doi.org/10.1002/adfm.202108977

Kryvenko, P., Rudenko, I., Konstantynovskyi, O. and Gelevera, O., Design, characterization, and incorporation of the alkaline aluminosilicate binder in temperature-insulating composites, *Mater.,* 17(3), 664 (2024). https://doi.org/10.3390/ma17030664

Li, X., Shen, C. and Yu, C. W., Building energy efficiency: Passive technology or active technology?, *Indoor Built Environ.,* 26(6), 729–732 (2017). https://doi.org/10.1177/1420326X17719157

Li, Y., Zhang, Y., Yang, Z., Xue, X., He, Z., Wang, H., Wang, C., Qu, J., Feng, Y., Zhang, W. and Xu, L., Waterborne coatings with sub-ambient cooling under direct sunlight–part I: Optical properties and cooling effect measurements, *Solar Energy Mater. Solar Cells,* 217, 110672 (2020). https://doi.org/10.1016/j.solmat.2020.110672

Liu, R., Wang, S., Zhou, Z., Zhang, K., Wang, G., Chen, C. and Long, Y., Materials in radiative cooling technologies, *Adv. Mater.,* 37(2), 2401577 (2025). https://doi.org/10.1002/adma.202401577

Liu, Y., Dai, C., Wang, K., Zou, C., Gao, M., Fang, Y., Zhao, M., Wu, Y. and You, Q., Study on a novel cross-linked polymer gel strengthened with silica nanoparticles, *Energy Fuels*, 31(9), 9152–9161 (2017). https://doi.org/10.1021/acs.energyfuels.7b01432

Mahrous, M. A., Abdelghany, M. A., Trindade, A. C. C., Aboukhatwa, M., Kriven, W. M. and Jasiuk, I. M., Investigating irradiation effects on metakaolin-based geopolymer, *Constr. Build. Mater.,* 437, 136837 (2024). https://doi.org/10.1016/j.conbuildmat.2024.136837

Meng, S., Long, L., Wu, Z., Denisuk, N., Yang, Y., Wang, L., Cao, F. and Zhu, Y., Scalable dual-layer film with broadband infrared emission for sub-ambient daytime radiative cooling, *Solar Energy Mater. Solar Cells,* 208, 110393 (2020). https://doi.org/10.1016/j.solmat.2020.110393

Mousavi, M. and Fini, E., Silanization mechanism of silica nanoparticles in bitumen using 3-aminopropyl triethoxysilane (APTES) and 3-glycidyloxypropyl trimethoxysilane (GPTMS), *ACS Sustainable Chem. Eng.,* 8(8), 3231–3240 (2020). https://doi.org/10.1021/acssuschemeng.9b06741

N'cho, W. C., Gharzouni, A., Jouin, J. and Rossignol, S., Impact of different metakaolin mixtures on oligomer formation and geopolymer properties: Impurity effect, *Open Ceram.,* 15, 100411 (2023). https://doi.org/10.1016/j.oceram.2023.100411

Naskar, S. and Chakraborty, A. K., Effect of nano materials in geopolymer concrete, *Perspect. Sci.,* 8, 273–275 (2016). https://doi.org/10.1016/j.pisc.2016.04.049

Ngouloure, Z. N., Kamseu, E., Moungam, L. M. B. A., Tchakoute, H. K., Valentini, L. and Leonelli, C., Design of porous geopolymers for hygrothermal applications: Role of nano and meso porosity, *Silicon*, 14(15), 10045–10059 (2022). https://doi.org/10.1007/s12633-022-01741-4

Niranjana, V. S., Ponnan, S., Mukundan, A., Prabu, A. A. and Wang, H. C., Emerging trends in silane-modified nanomaterial–polymer nanocomposites for energy harvesting applications, *Polym.,* 17(10), 1416 (2025). https://doi.org/10.3390/polym17101416

Qu, J., Zhang, J., Li, H., Li, S., Hou, X., Chang, R. and Zhang, Y., Coal gasification slag-derived highly reactive silica for high modulus sodium silicate synthesis: Process and mechanism, *Chem. Eng. J.*, 479, 147771 (2024). https://doi.org/10.1016/j.cej.2023.147771

Rees, C. A., Provis, J. L., Lukey, G. C. and van Deventer, J. S. J., Attenuated total reflectance Fourier transform infrared analysis of fly ash geopolymer gel aging, *Langmuir*, 23(15), 8170–8179 (2007). https://doi.org/10.1021/la700713g

Safdar, A., Mohamed, H. E. A., Muhaymin, A., Hkiri, K., Matinise, N. and Maaza, M., Biogenic synthesis of nickel cobaltite nanoparticles via a green route for enhancing the photocatalytic and electrochemical performances, *Sci. Rep*., 14(1), 17620 (2024). https://doi.org/10.1038/s41598-024-68574-6

Sujitha, V. S., Ramesh, B. and Xavier, J. R., Effects of silane-functionalized nanocomposites in superabsorbent polymer and its reinforcing effects in cementitious materials, *Polym. Bulletin,* 81(4), 3479–3512 (2024). https://doi.org/10.1007/s00289-023-04888-1

Tran, N. P. and Ngo, T. D., Thermal degradation of copper-modified geopolymer containing graphene oxide under cyclic heating, Constr. Build. Mater., 489, 142194 (2025). https://doi.org/10.1016/j.conbuildmat.2025.142194

Veloso, R. C., Souza, A., Maia, J., Ramos, N. M. M. and Ventura, J., Nanomaterials with high solar reflectance as an emerging path towards energy-efficient envelope systems: A review, *J. Mater. Sci.,* 56(36), 19791–19839 (2021). https://doi.org/10.1007/s10853-021-06560-3

Vignesh, J., Ramesh, B. and Xavier, J. R., A comprehensive review of materials, processing, and performance of nano-doped engineered geopolymer composites for construction applications, *Case Stud. Constr. Mater.,* e05625 (2025). https://doi.org/10.1016/j.cscm.2025.e05625

Wen, L., Xu, J., Yang, Q., Zhang, F., Li, F. and Zhang, L., Gelation process of nanosilica sol and its mechanism: Molecular dynamics simulation, *Chem. Eng. Sci.,* 216, 115538 (2020). https://doi.org/10.1016/j.ces.2020.115538

Woźnica, M., Sobiech, M. and Luliński, P., A fusion of molecular imprinting technology and siloxane chemistry: A way to advanced hybrid nanomaterials, *Nanomater.,* 13(2), 248 (2023). https://doi.org/10.3390/nano13020248

Yang, L., Hu, X., Liu, Y., Zhou, D., Yuan, B., Liu, S., Luo, Z., Li, X., Jin, D. and Xu, F., Multiscale characterization of geopolymers modified with alkali-catalyzed nanosilica: Effects on dispersion and mechanical properties, *Cem. Concr. Compos.,* 165, 106324 (2025). https://doi.org/10.1016/j.cemconcomp.2025.106324

Ziada, M., The effect of nano-TiO_2 and nano-Al_2O_3 on mechanical, microstructure properties and high-temperature resistance of geopolymer mortars, *Arabian J. Sci. Eng.,* 50(16), 12977–12996 (2025). https://doi.org/10.1007/s13369-024-09570-w

Zidi, Z., Ltifi, M. and Zafar, I., Synthesis and attributes of nano-SiO_2 local metakaolin-based geopolymer, *J. Build. Eng.,* 33, 101586 (2021). https://doi.org/10.1016/j.jobe.2020.101586